49th AIAA Aerospace Sciences Meeting including the New Horizons Forum and Aerospace Exposition
4 - 7 January 2011, Orlando, Florida

Pyrolysis gas flow in thermally ablating media using time-implicit discontinuous Galerkin methods

Ankush Bhatia[1] and Subrata Roy[2]
Applied Physics Research Group, Department of Mechanical and Aerospace Engineering, University of Florida, Gainesville, FL – 32611, USA

Ryan Gosse[3]
Center of Excellence, Air Force Research Laboratory, AFRL/RBAC, Bldg 146B, 2210 Eighth St., WPAFB, OH 45433-7512, USA

In this work, we apply time-implicit discontinuous Galerkin methods to the problem of thermal ablation, where we solve for the dynamics of flow of pyrolysis gas in a charring ablating media. We have benchmarked our results with the published data. The protective coating of thermal protection system over the space vehicle is of the order of a few centimeters, and high flow speed of gas and dominant source terms in the problem put very restrictive CFL limit necessitating the use of implicit time integration methods. Good convergence of these methods is ensured by use of Newton method, where the required jacobians are calculated numerically for accurate evaluations. Analytical approach to evaluate the jacobians, especially for thermal ablation problems, is very cumbersome, and causes serious convergence issues. We have also tested our development of DG capability for 2-D double Mach reflection problem for extending the code to 2-D thermal ablation in future.

Nomenclature

α	=	maximum eigenvalue
c	=	speed of sound
Cp_c	=	specific heat of char
Cp_r	=	specific heat of resin
D	=	diffusion term for pyrolysis gas
e_c	=	internal energy of char
e_g	=	internal energy of gas
e_r	=	internal energy of resin
ε	=	void fraction
f	=	friction term
h_r^o	=	heat of formation of resin
I	=	Inertia
k	=	thermal conductivity
K_g	=	permeability
λ	=	eigenvalue
μ	=	viscosity of gas
ρ	=	density

I. Introduction

Space vehicles upon entry into a planet's atmosphere typically experience high heat fluxes to their surface. Excessive heat flux results from combined effect of convective and radiative components. Chemical reactions of

[1] Graduate student, student member, AIAA
[2] Associate Professor, Associate Fellow, AIAA
[3] Research Engineer, AIAA Member

the dissociated and ionized gas species (present in the shock layer, which is between the bow shock and boundary layer) also add on to the overall heating of the surface. Thus, role of a protective coating on the vehicle's surface, called Thermal Protection System (TPS) is critical for the successful and safe entry of the space vehicle. Thermal ablation refers to the mechanism by which ablating TPS undergo degradation at high temperatures, and reject high heat-content material at the surface itself thus shielding the vehicle from the effect of immense surface heating. In addition, charring type ablators undergo thermal decomposition (of resin component) within and release mixture of gases called pyrolysis gas into the boundary layer. These gases provide further cooling of the medium both by absorbing the heat from the material and by pushing the incoming hot gases (from the flow over the vehicle) away from the surface, thus providing a reduction in overall convective heating.

Problem of thermal ablation is crucial to the success of TPS design studies, where the goal is to accurately predict the response of TPS, to given flow conditions, to arrive at an optimum mass, size and shape for the TPS. Mass of TPS is directly linked to the launching cost of the vehicle, and its size and shape to the aerodynamic coefficients of lift and drag. Thermal ablation is a very complex, highly non-linear and fully coupled multi-physics problem. In addition to this, TPS for larger and more advanced payloads are no longer a simple geometry, single piece of material, but a complicated geometry and consists of layers of stacked and multiple materials. Most of the thermal response codes developed so far are based on finite difference and finite volume methods and are limited to simple geometries. Finite element method has so far been limited to only conduction part of the problem, where no ablation is considered. Also most of the codes neglect the flow of pyrolysis gas within ablating media missing on its effect on the overall response of TPS, as shown in various studies. Capability of finite element methods to accommodate complex geometries (by use of unstructured meshes), ability to conveniently apply difficult boundary conditions (typical of thermal ablation problem at the interface of solid and fluid domain) without any loss of accuracy at the boundary, and scalability for parallel architectures (due to its compact scheme even for higher order schemes) make it particularly suitable for thermal ablation problem.

Discontinuous Galerkin (DG) methods combine the advantages of both finite element and finite volume methods. They were formally developed for hyperbolic conservation laws by Cockburn and Shu [3-6] and later on applied to elliptic or convection-diffusion type of problems [7-10]. In work by Persson and Peraire, they have been applied to various problems of viscous flows, shocks, turbulent flows and computational aeroacoustics [11-15, 27] to make them practical for problems of practical interest. We extend the application of discontinuous Galerkin methods to the field of thermal ablation. As a first step, we solve an Arc jet case (a 1-D thermal ablation problem) given in Wakefield and Pitts, 1980 [20] and later on simulated by Ahn and Park in their two papers in 1998 and 2002 [1, 2].

As pointed out in [1] and [2], numerical codes for solving thermal ablation problem assumes the flow of pyrolysis gas generated upon decomposition of resin material to be steady state. Such an assumption is valid for high heating rate environment and high pressure, wherein the gas leaves the system as soon as it is generated. Thus, there is no need to solve for the flow of pyrolysis gas within the porous media. However such an assumption is not valid in moderate to low heating environments. The governing equations of the flow for such environment are as given in [2],

$$\frac{\partial \rho_r}{\partial t} = -R \tag{1}$$

$$\frac{\partial \left(\varepsilon \rho_g\right)}{\partial t} + \frac{\partial \left(\varepsilon \rho_g u\right)}{\partial x} = R + D \tag{2}$$

$$\frac{\partial \left(\varepsilon \rho_g u\right)}{\partial t} + \frac{\partial \left(\varepsilon \rho_g u^2 + \varepsilon P\right)}{\partial x} = -\varepsilon f + I \tag{3}$$

$$\frac{\partial}{\partial t}\left(\rho_c e_c + \rho_r e_r + \varepsilon \rho_g e_g + \frac{1}{2}\varepsilon \rho_g u^2\right) + \frac{\partial}{\partial x}\left[\varepsilon u\left(\rho_g e_g + \frac{1}{2}\rho_g u^2 + P\right)\right] = \frac{\partial}{\partial x}\left(k\frac{\partial T}{\partial x}\right) \tag{4}$$

where,

$$\varepsilon = \varepsilon_{\max} - \rho_r / \rho_p \tag{5}$$

$$R = \sum_{k=1}^{N} A_k \exp\left(-\frac{B_k}{T}\right)\rho_v \left(\frac{\rho_r}{\rho_v}\right)^n \tag{6}$$

$$D = \frac{K_g}{\mu}\left(\varepsilon\rho_g\right)\varepsilon\frac{\partial^2 P}{\partial x^2} \tag{7}$$

$$f = \left(\frac{\mu}{K_g}\right)u \tag{8}$$

$$I = 1.222\left(\frac{1}{\sqrt{K_g}}\right)\rho_g u^2 \tag{9}$$

In the above equations, Eq. (1) defines the decomposition of resin material. Here ρ_r is resin density and R is decomposition rate dependent on temperature, T and the resin density, ρ_r, given in Eq. (6). The Eq. (2) solves for conservation of mass for gas density, here ε is void fraction and is given by Eq. (5). Here, ε_{max} is maximum void fraction that happens in char state, and ρ_p is intrinsic density of resin and both their values are equal to 0.1788 and 1763.6 kg/m3. Opposite signs for R in first two equations (1) and (2) indicates that resin decomposes to release pyrolysis gas. Second term, D on right hand side of Eq. (2) is the diffusion term that represents the rate of change of gas density due to the spatial variation of pressure, and is given by Eq. (7). In this expression, K_g is the permeability of gas, and μ is gas viscosity. Eq. (3) governs the momentum conservation of the gas. Flow of the gas is pressure driven. Here u is the gas velocity and $\varepsilon\rho_g u$ is the gas momentum. Since the gas is flowing through the porous media, the resistance to gas motion are given through f, friction and I, Inertia terms given in equations (8) and (9) respectively. The Eq. (4) solves for combined energy conservation of both solid (resin + char) and gas. First term in Eq. (4) gives unsteady variation of total energy, E, of the system. e_g, e_c, and e_r are internal energies of the gas, char and resin material respectively. Second term in Eq. (4) is derivative of energy flux, similar to Euler equations, where the flux is decided by internal and kinetic energy and pressure flow energy of gas. These terms were neglected in most thermal response codes since the gas was supposed to leave the material as soon as it was generated. Last term in energy equation is heat conduction within the material, through which we also apply net heat flux boundary condition at the surface. The terms, e_c and e_r, are evaluated using specific heats of both materials (char and resin) and are given as,

$$e_C = \rho_C C_{pc} T \tag{10}$$

$$e_r = \rho_r C_{pr} T + \rho_r h_r^o \tag{11}$$

Specific heat for solid carbon char, Cp_c used in Eq. (10) is given as,

$$C_{pc}(T) = c_1 z^4 + c_2 z^3 + c_3 z^2 + c_4 z + c_5 \frac{J}{Kg.K} \tag{12}$$

Here, $z = \log_{10}T$, $c_1 = -6.5$, $c_2 = -143.7$, $c_3 = 706.7$, $c_4 = 1835$ and $c_5 = -5700$. Specific heat for resin material, Cp_r is assumed to stay at constant value of 1174 W/m-K. This value wasn't provided in [1, 2]. We consider two cases for above given governing equations, as done in [1] and [2]. The differences between both cases are highlighted in Table 1. Papers, [1] and [2] use two different models for friction term, f, which have different magnitudes. It was

found that the friction term in [1] is two orders of magnitude higher than friction term in [2]. Both use two different values of thermal conductivity and there's no Inertia term considered in [1]. Also, Diffusion term, D, is missing in the equations given in [1]. All these major differences in two papers are summarized in Table 1. This table lists friction, f, conductivity, k, Inertia, I and diffusion coefficient, D.

Table 1: Differences in modeling terms in [1] and [2]

Difference #	1998 paper, [1]	2002 paper, [2]
1	$f = 7.8 \text{ X } 10^{7}(T/300)^{0.75}(\varepsilon/0.1788)u$	$f = 2.58 \text{ X } 10^{5}(T/500)^{.769}(\varepsilon^{.381})u$
2	$\text{Log}_{10}k(T) = -6.343X10^{-9}T^{2} + 3.97X10^{-4}T - 0.193$	$\text{Log}_{10}k(T) = -6.5X10^{-8}T^{2} + 5X10^{-4}T - 0.1$
3	$I = 0$	$I = (1.222/K_{g}^{0.5})\rho_{g}u^{2}$
4	$D = 0$	$D = (K_{g}/\mu)(\varepsilon\rho_{g})\varepsilon\partial^{2}P/\partial x^{2}$

The work in these papers was a reasonable starting point for us to test our DG formulation anchored in MIG, Multi-scale Ionized Gas flow Code, which is a family of our in-house finite element modules, and has been used to solve problems in plasma dynamics like low pressure Hall thruster, high pressure RF induced optical glow discharges, and microthrusters, microchannel and nanopore flows etc.[16-19] We have also worked in building a 2-D DG capability to use them later on in 2-D Thermal Ablation problems.

II. Full Model Description

We consider an Arc-jet problem simulated by Wakefield and Pitts[20] and Ahn and Park[1, 2]. The TPS is exposed to a heat flux of 1400 W/cm^2. The problem is 1-D with domain thickness of 1 cm. As the heat flux transfers into the material through thermal conduction, the resin material undergoes decomposition and produces a mixture of gases, known as pyrolysis gas. 14 gas species are considered, C, CH, CH_2, CH_3, CH_4, CO, CO_2, C_2, C_3, H, HO, H_2O, O, and O_2. These are taken to be at thermal equilibrium at the temperature of the solid material and pressure of the gas inside the porous media. Equilibrium properties of the gas mixture, like molecular weight, internal energy and pressure are evaluated using an external thermo-chemical solver, CANTERA[21]. The properties are expressed as a function of temperature and gas density. Further details on thermo-chemical modeling used in CANTERA were already discussed in our earlier paper, [24]. We have used two curve fits for internal energy, e_g (see Fig. 2). First curve fit, (green curve) is a single exponential curve for the complete range of temperature between 200 K and 3400 K. This curve under predicts internal energy for temperature range from 2400 K to 3000 K and over predicts from 3000 K to 3400 K. For temperature range below 3000 K, this under-prediction of internal energy is significant, and results in lower prediction of cooling provided by the flow of gas. Therefore for more accurate prediction we pick second curve as shown in Fig. 2. This curve is blue exponential curve from 200 K to 2800 K and black exponential curve from 2800 K to 3400 K. The expressions of both internal energy, eg and molecular weight, MW are given as,

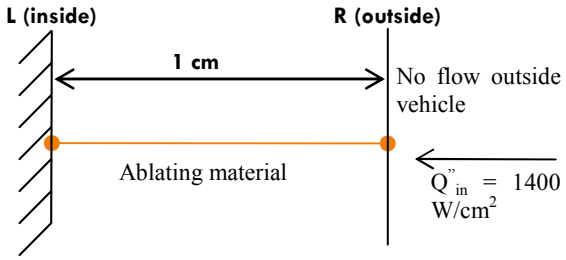

Figure 1. Schematic of 1-D thermal ablation problem (material is carbon phenolic)

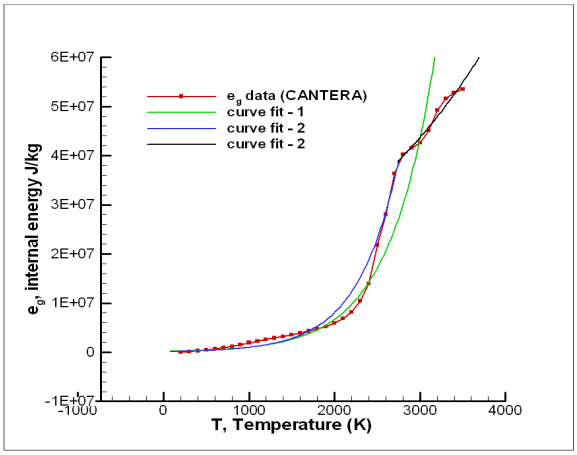

Figure 2. Plot of internal energy, e_g, with Temperature, T, for pyrolysis gas, comparing two curve fits, #1 and #2. Out of both curve fit – 2 is more accurate.

$$e_g = \exp\left(A_1 T + A_2\right) - A_3 \tag{13}$$

$$MW = B_1 \exp(y) + B_2 \exp(x) + B_3 \exp(x)\exp(y) + B_4 \tag{14}$$

Here, A_1 = 1.869e-03, A_2 = 1.198exp+01 and A_3 = 1.156exp+07. For Eq. (14), x and y depend on temperature and gas density respectively as, x = $(T/1000)^2$ and y = $LOG_{10}(\rho_g)$, and constants are B_1 = 1.7981exp-04, B_2 = -1.333exp-06, B_3 = 2.0159exp-07, and B_4 = 1.678exp-02.

Due to gas generation and increase in temperature, the pressure of gas rises within the domain which causes the gas to leak out to the atmosphere. This gas as shown in the results section leaks out to the atmosphere with velocities of order of 100 m/s, and within the material domain they have velocities close to 20 – 40 m/s, which causes sufficient cooling within the material domain, while it is ablating. This effect is neglected in other numerical works in thermal ablation.

III. Numerical Scheme (Discontinuous Galerkin Method)

We initially attempted the above described thermal ablation problem with Galerkin based finite element method. This method develops spurious oscillations in the solution and is unable to capture solutions with high gas velocities. Discontinuous Galerkin method allows for the solution to be discontinuous across element boundary and thus can accommodate for solutions with steep gradients and high gas velocities. The in-built dissipation mechanism of DG methods results from the use of approximate numerical fluxes for the inviscid fluxes. This in-built dissipation is proportional to the jump in the solution across solution variable. Hence DG methods are suitable to treat flows with high speeds. DG methods were developed by Cockburn and Shu, as a class of explicit methods, called TVD Runge-Kutta Discontinuous Galerkin method (TVD RKDG), in their series of papers from 1989 – 2001[3–6]. They have been applied to various problems like Compressible flow, Navier Stokes, electro-hydrodynamics, computational aeroacoustics, turbulent flows, flapping wings etc[7, 11-15]. Persson and Peraire have worked on applying time-implicit DG methods to more practical and real world problems, and some of their work include areas like development of Compact Discontinuous Galerkin (CDG) scheme, preconditioners for time-efficient solution of matrix-systems obtained from application of DG methods, sub-cell shock capturing by artificial dissipation for capturing flows with shock, and using high order DG methods to capture shock within one element etc [11 – 15]. Their work is very relevant to us in the development of implicit DG method for thermal ablation problems.

A. 1-D Discontinuous Galerkin method

As a first step, we developed explicit RKDG and DG methods. Such explicit schemes are insufficient for thermal ablation problems as they pose heavy restrictions on CFL number. For example, for the 1-D thermal ablation, maximum time-step that could be used for the explicit DG methods was 1.0×10^{-08} sec. Total run time for thermal ablation problems is however usually on the order of few seconds. Therefore explicit schemes are highly insufficient for solving thermal ablation problems, even for a 1-D case. The situation worsens for higher dimensions. The severity of restriction on CFL numbers increases as the domain size decreases, and net amount of gas flow velocity and source terms increase in the problem. Implicit DG methods allow for higher time-steps, e.g. in our current 1-D thermal ablation problem we were able to use time step as high as 1.0×10^{-03} sec, which corresponds to a CFL number of around 1000. Since source terms are very large, we also get a highly ill conditioned matrix, which needs to be solved using preconditioners. A brief derivation of the weak form of discontinuous Galerkin methods with implicit time integration for a general governing equation in Eq. (15) follows below.

$$\frac{\partial U}{\partial t} + \frac{\partial F(U)}{\partial x} + \frac{\partial F_v(U, \nabla U)}{\partial x} = G(U) \tag{15}$$

Here, U is solution vector, F (U) is inviscid flux vector, F_v (U, ∇U) is viscous flux vector, and G (U) is source vector. Approximation of solution vector U is written in terms of basis function, ϕ^l_j and degree of freedoms U^i_j as written in Eq. (16). Substituting Eq. (16) in Eq. (15) and multiplying resultant equation by a test function ϕ^l_j gives us a weak form. Upon integration by parts to both the inviscid and viscous flux terms, the weak form is given by Eq. (17). The coefficient of the first term in Eq. (17), is the mass matrix, M given in Eq. (18).

$$U \equiv U_j = \sum_{l=0}^{k} \phi_j^l U_j^l \tag{16}$$

$$\left[\int \{\phi\}\{\phi\}^T dx\right]\frac{\partial\{U_j^l\}}{\partial t} - \int\left\{\frac{\partial\phi}{\partial x}F\right\}dx + |\phi.F|_-^+ - \int\left\{\frac{\partial\phi}{\partial x}F_v\right\}dx + |\phi.F_v|_-^+ = \int\{\phi G\}dx \tag{17}$$

$$[M]\left[\frac{\{U_j^l\}^{n+1} - \{U_j^l\}^n}{\Delta t}\right] = \int\left\{\frac{\partial\phi}{\partial x}F\right\}dx - |\phi.F|_-^+ + \int\left\{\frac{\partial\phi}{\partial x}.F_v\right\}dx - |\phi.F_v|_-^+ + \int\{\phi.G\}dx \tag{18}$$

We have used Legendre polynomials for the basis functions, which leads to a diagonal mass matrix. Overall Jacobian matrix obtained is structured in block-wise fashion and thus is amenable to parallelization for faster computations. This task shall be taken up in the future work. For approximation of numerical fluxes we have used Local Lax Friedrichs (LLF) flux for inviscid fluxes and BR-1 (Bassi Rebay – 1) for viscous fluxes in equations 19 and 20. As a standard practice, we use auxiliary equations to deal with viscous terms in DG method.

$$H^{LLF}(a,b) = \frac{1}{2}\left(F(a) + F(b) - \alpha(b-a)\right)$$

$$\alpha = \max_{\min(a,b)\le s\le\max(a,b)}\left|\frac{\partial F}{\partial U}(s)\right| \tag{19}$$

$$H_v(a,b) = \frac{1}{2}\left(F_v(a) + F_v(b)\right) \tag{20}$$

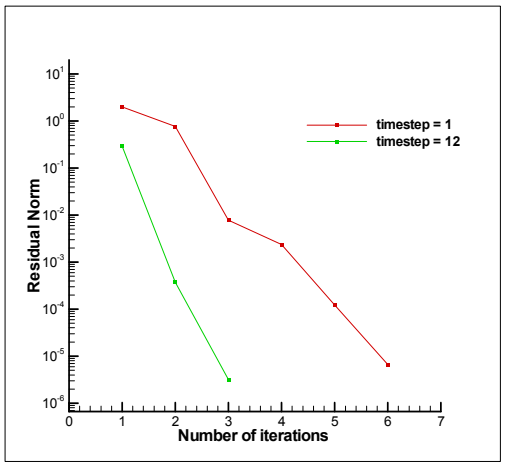

Figure 3. Residual convergence plot for a test case designed for thermal ablation problem and time-step of 1.0e-06 sec. Plot shows near quadratic convergence of the scheme.

Since problem is non-linearly coupled, we use Newton's method to solve the implicit system and fast convergence of the method depends on the accurate evaluation of Jacobian. Our initial attempt was at getting the analytical expressions of the Jacobians. We have already demonstrated complexity and limitations that abound analytical approach to evaluate jacobians in [24] and [28]. To summarize, approach of evaluating analytical expressions is very cumbersome, and has convergence and stability problems for thermal ablation. It's also not generalized and typically requires a lot of work for a new given problem. For any new problem, new analytical expressions need to be found, and such expressions become large and difficult to handle. This approach is also more prone to errors. Also, Jacobian evaluation at the boundary is crucial, e.g. if a variable at the boundary is fixed, then while calculating Jacobian, it should be treated as constant when differentiating w. r. t. other variables; and differentiation w. r. t. the fixed variable should not be considered. Due to all the above reasons we took to numerical approach to evaluate these jacobians, which proved to be much more accurate, effective and convenient to use. This approach is also not dependent on the given system of equations and is thus general in application. We don't need to change this part of code for any system of equations. For numerical approach of evaluating jacobians, we perturb a solution variable and then calculate the change in flux term that it produces. By applying simple finite difference we get a first order approximation to the Jacobian, which is accurate enough if the perturbation is sufficiently small. Due to coupling between elements (through derivatives of F^+ and F^-), and numerical evaluation, we were able to achieve near quadratic convergence for thermal ablation problems as shown in Fig. 3.

B. 2-D Discontinuous Galerkin method

For the time integration of 2-D Discontinuous Galerkin method, we use implicit scheme. 2-D model problem is given by Eq. 21, where F and F_v have x and y components. Multiplying Eq. 21 by a test function and integrating over domain (along with integration by parts for viscous and inviscid flux terms) gives us weak form in Eq. 22.

$$\frac{\partial U}{\partial t} + \nabla . F_i\left(U\right) - \nabla . F_{\mathrm{v}}\left(U, \nabla U\right) = G \tag{21}$$

$$\int_E \left(v \frac{\partial U}{\partial t} \right) d\Omega + \oint_{\partial E} vF . \vec{n} d\sigma - \int_E \nabla v . F d\Omega - \oint_{\partial E} vF_v . \vec{n} d\sigma + \int_E \nabla v . F_v d\Omega - \int_E vG d\Omega = 0 \tag{22}$$

Basis functions chosen for the above formulation are Jacobi polynomials, and are given in Table 2 below. These basis functions were taken from [25]. Here, coordinates x and y are given for a reference square element, which can be transformed to a general quadrilateral in the physical space using bilinear mapping. These basis functions are orthogonal, and thus the mass matrix will be diagonal, but since we allow general quadrilaterals whose opposite sides may not be parallel, therefore the Jacobian of transformation will no longer be independent of position within the reference element, and hence we will have a mass matrix that will no longer be diagonal, but symmetric.

Table 2: Basis functions expressions based on their orders. Here x and y are coordinates for the reference geometry which maps to a generalized quadrilateral.

Basis/Order	1	2	3	4
1	1	1	1	1
2		-1+2x	-1+2x	-1+2x
3		-1+2y	-1+2y	-1+2y
4			$1-6x+6x^2$	$1-6x+6x^2$
5			1-2y-2x+2xy	1-2y-2x+4xy
6			$1-6y+6y^2$	$1-6y+6y^2$
7				$-1+12x-30x^2+20x^3$
8				$-1+2y+6x-12xy-6y^2+12xy^2$
9				$-1+6y-6y^2+2x-12xy+12yx^2$
10				$-1+12y-20y^2+20y^3$

IV. Results and Discussions

We present results for 1-D thermal ablation problem that was described in section III and also demonstrate our development of 2-D discontinuous Galerkin methods and its application to a double mach reflection problem. Before presenting these results and the discussion that follows, we validate our DG code for a 1-D Sod's shock tube problem, comparing results with the analytical solution.

A. Validation case for discontinuous Galerkin method

We validate results for a shock tube problem with a test case from Toro [29]. Sod's shock tube is a well known problem and its analytical solution is also available for test of accuracy and convergence. Total domain length is 1 m, and is divided into two chambers, left and right at x = 0.5 m. Initial values for density and pressure in left chamber are both 1 in SI units, and in right chamber are 0.125 and 0.1 respectively. Velocity is initialized to a zero value. The solutions are plotted at total time of 0.2 sec.

This case is run using implicit DG code with time-steps of 1.0×10^{-3} and 1.0×10^{-4} sec. We use local Lax-Friedrichs for numerical fluxes, and show comparison of solutions of order of accuracy up to 4 (LLF 01-04) for the code with the exact solution in Fig. 4. Solution accuracy is definitely improved at a lower time-step. Implicit time-integration scheme has also has its own dissipation mechanism, which can be seen in smearing of solution and oscillation peaks with time step of 1.0×10^{-3} sec. We also provide close-ups of three regions namely, expansion fan,

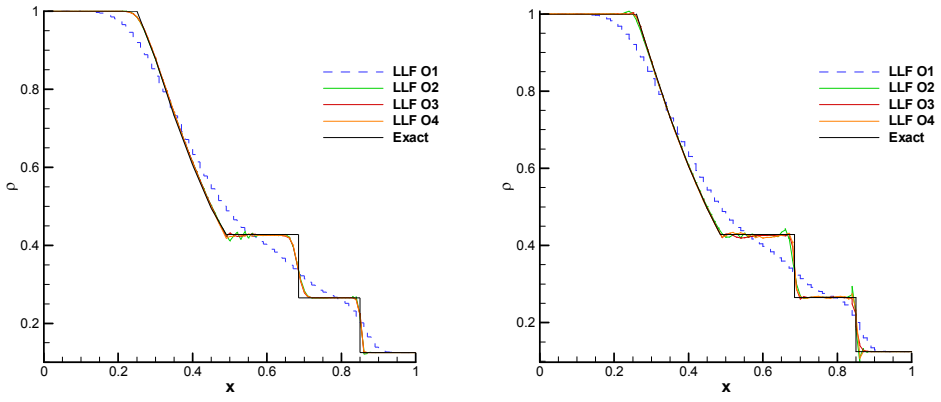

a) $\Delta t = 1.0\times10^{-03}$ sec **b) $\Delta t = 1.0\times10^{-04}$ sec**

Figure 4. Validation cases for shock tube problem for two time steps, a) 1.0e-03 sec and b) 1.0e-04 sec. Solution from DG simulations for high order accuracy is compared to exact solution, and higher accuracy gives closer solution.

contact discontinuity and shocks to give a better idea of how solution approximations improve with order of accuracy at each of these zones. These results are shown in Fig. 5 for time-step of 1.0×10^{-4} sec.

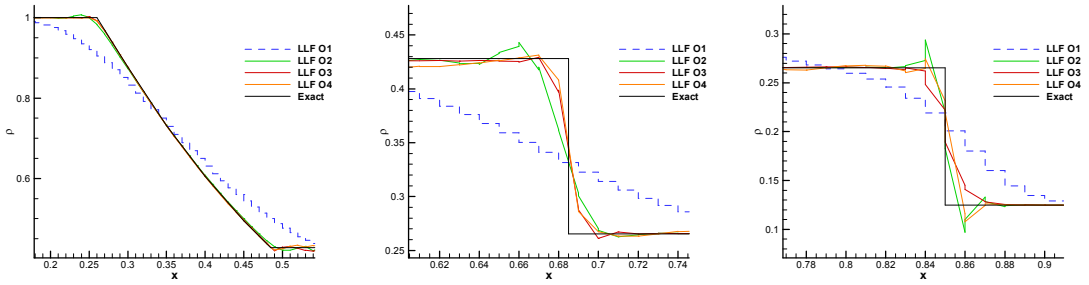

a) Expansion wave **b) Contact discontinuity** **c) Shock wave**

Figure 5. Close ups of three regions in shock-tube, a) expansion wave, b) contact discontinuity and c) shock wave. Time step for above simulations is 1.0×10^{-4} sec. Higher polynomial approximations lead to more accurate results.

B. 1-D thermal ablation using discontinuous Galerkin method

An Arc-jet wind tunnel experiment was conducted in [20] with a carbon-phenolic sample that was exposed to a heat flux of 1400 W/cm^2. Experiment results were compared with simulation results from Charring Material Ablation code or CMA. Later on, these results were also published in [1] and [2]. Total run time for this problem is 5 sec, and surface pressure and enthalpy at the exit are 0.22 atm and 23300 J/g. Total thickness of the test sample is 1 cm.

Here we consider two cases, as taken in [1] and [2]. Differences in both these cases were noted in the introduction section. To compare the effect of diffusion term modeling between both the cases, we use friction term and thermal conductivity from [2] in both the cases. First we present results obtained for the case with D = 0, which was considered in [1]. In Fig. 6 a) and b), we show spatial distribution of solution variables at a time of 4 sec. It can be seen from plot of resin density, ρ_r that pyrolysis zone extends from 2 mm to 4 mm. Other 2 zones, i.e. virgin plastic (ρ_r = 250 kg/m^3) and char zone (ρ_r = 0 kg/m^3) can also be identified from this plot. Pressure varies from a value of nearly 8 atm in the region of virgin plastic, where it is flat, to a low 0.22 atm at the right side of domain. High pressure gradient of the gas is observed within the pyrolysis zone. The gas flow is actually driven by the gradient of the product of the gas pressure, P and void fraction, ε. This is seen in the jump of velocity magnitude in the pyrolysis zone, and higher velocities are attained at the right boundary due to a steeper gradient of εP. We also observe some numerical artifacts in the solution of gas momentum, possibly due to dominant friction term in Eq. (3). Cooling effect of pyrolysis gas can also be seen from these plots.

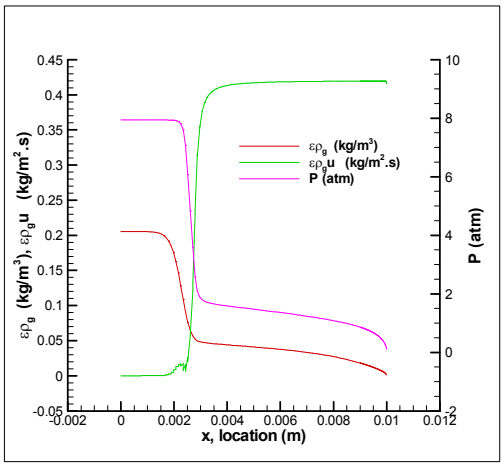

a) Gas density, gas momentum and pressure

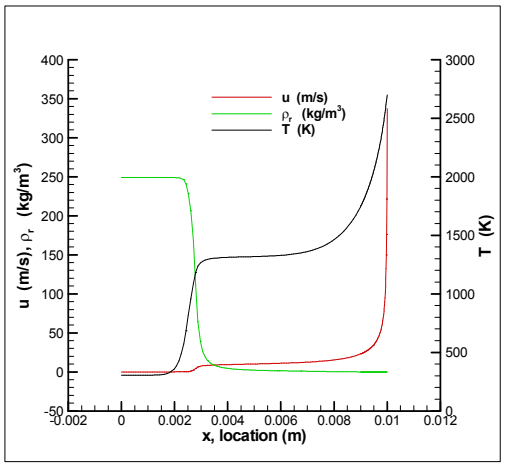

b) Gas velocity, resin density and temperature

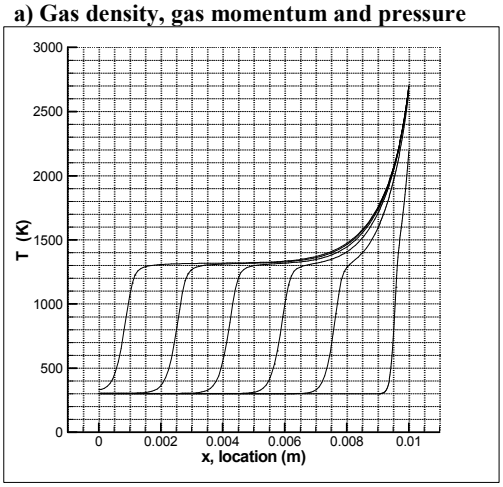

c) Temperature distribution at different times

Figure 6. Top two plots a) and b) show all solution variables for Arc-jet case with D = 0 at time = 4 sec. a) shows gas density, $\varepsilon\rho_g$, gas momentum, $\varepsilon\rho_g u$ and pressure, P; b) shows gas velocity, u, resin density, ρ_r, and temperature, T; and c) shows temperature distribution within the domain at times = 0.1, 1, 2, 3, 4, and 5 sec.

Temperature distribution within the material has steeper gradient at the pyrolysis front, seen at around 2 mm in Fig. 6b), as compared to elsewhere in domain. There are two heating mechanisms in the domain, thermal conduction and convection cooling. In beginning of pyrolysis zone, we expect thermal conduction to be the dominant phenomena, whereas at other places in the char we expect both convection cooling and conduction to play an equally important role. This explains the observed temperature distribution and the trend of thermal response (at different times) that can be seen in Fig. 6c), where a steep rise in temperature is slowed down by the convection cooling of the exiting pyrolysis gas. Based on our calculations, we find that temporal increase in pyrolysis gas density in the virgin plastic zone (region to the left of pyrolysis zone) is due to resin decomposition rate, R, which also leads to corresponding gas generation. The temperature in the virgin zone is 300 K, so value of R should be very close to zero, which is not the case with the model for R given in [1] and [2]. Based on these calculations, we come to conclusion that all the gas that is generated during pyrolysis (in the pyrolysis zone) primarily leaves out to the atmosphere. Both friction and inertia terms in [2] provide resistance to the flow of gas. Higher values for friction term in [1] results in higher resistance to the flow and hence larger gas density values are observed within the virgin plastic domain. This would result in higher pressure to be observed for [1] as compared to [2]. This difference was noted in the pressure results reported in [1] and [2]. Gas pressure for the day probe in the virgin plastic domain is nearly 75.67 atm for [1] and 30 atm for [2] at a flight time of 27 sec. We are investigating this difference in two models between 2 papers. We will note here that we have used friction model from [2] for both the cases that we ran, to compare the effect of Diffusion term alone between both the cases.

In Fig. 7, we compare our results for temporal variation of surface temperature (on the right side of domain shown in Fig. 1). We provide results for our simulation for both curve fit – 1 and curve fit – 2 for internal energy, e_g. As we have already mentioned that curve fit – 2 is more accurate than curve 1, we find that our results match the

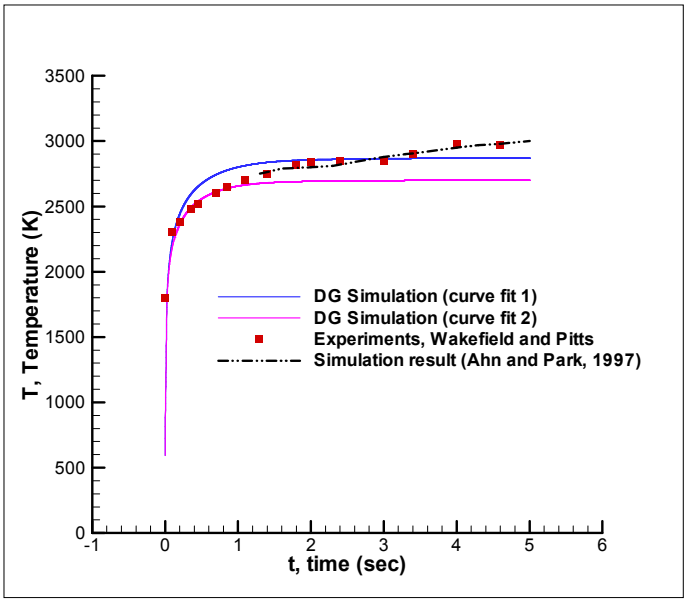

Figure 7. Temporal variation of surface temperature for DG simulation with D = 0, and comparison with 1998 paper and experimental results.

experimental results for initial 1 sec, and after that due to high gas velocity, there's no further rise in temperature observed. High gas velocity leads to high cooling at the surface, which exactly balances out net heat influx to the surface and thermal conduction.

Second case that we present is with nonzero diffusion term ($D \neq 0$) in Eq. 2. This case is exactly similar to [2]. Shown below in Fig. 8, are results for solution variables at time of 4 seconds. We now highlight the differences in both the cases, with and without diffusion term. Diffusion term in momentum equation is related to the second derivative of gas pressure, and results in more diffused profile for gas density. Pressure is related to gas density and temperature, and both are more diffused out, which causes a lower pressure (actually εP) gradient that drives the flow, and therefore we get lower gas momentum near exit, as compared to case D = 0. Therefore we find these results are consistent with basic gas dynamics.

Due to diffusion term, gas velocity at the point of gas generation is lower, and hence gas density is higher compared to case with D = 0 in the pyrolysis zone. Larger gas density absorbs more heat from the material, and hence temperatures at pyrolysis zone are lower for this case. This in turn affects the decomposition of resin material and we see a broader pyrolysis zone in this case, which extends roughly from 3 mm to 7 mm. This diffusion mechanism is in general better for the vehicle's body since it provides for more time that the vehicle gets before its temperature starts to increase. For example, temperatures above 500 K are observed at location of 2.25 mm for earlier case (D = 0) and for this case at location of 3.17 mm at time of 4 sec. There's no significant difference in pressure for both cases, pressure in this case is approximately 0.5 atm higher than that of case – 1. Velocities in the domain for this case are lower as compared to case with D = 0, therefore we have lower cooling within the domain, and since heat conduction is a diffusion mechanism, we observe more diffused profiles of temperature. So, from looking at temperature profile we can tell which effect is dominant, conduction or convective cooling.

We also show comparison of results obtained for both D = 0 and $D \neq 0$ at final time of 5 sec below in Fig. 10, and we can easily see that lesser amount of resin material is used for the case with $D \neq 0$ (top left plot in Fig. 10). The pyrolysis zone is identified from 0.002 m to 0.006 m for non-zero diffusion case, and that for zero diffusion from 0.0005 m to 0.0025 m; therefore pyrolysis zone is twice wide for non-zero diffusion case. Also, the pyrolysis front for non-zero diffusion case travels at lower speed than case with zero diffusion. Since temperatures around the pyrolysis zone are lower for non-zero diffusion than temperatures around pyrolysis zone for zero diffusion, net decomposition rate for non-zero diffusion case is lower, hence speed of pyrolysis front is slower. Lower speeds for exiting gas within the domain can be seen in Fig. 10 for non-zero diffusion and hence larger gas densities, which means more absorption of heat from the material and that is the reason why we observe lower and more diffused temperature plots.

Temporal variation of surface temperature with simulation results by [2] and experimental results by [20] are given in Fig. 9. Again we plot the results for both curve fits – 1 & 2 for internal energy. Our surface temperature

shoots to higher value at later time than experimental results. Reason for this as already explained is lower cooling for this case. (Given our lack of clarity about some aspects of their model, our plot is close to experiment results)

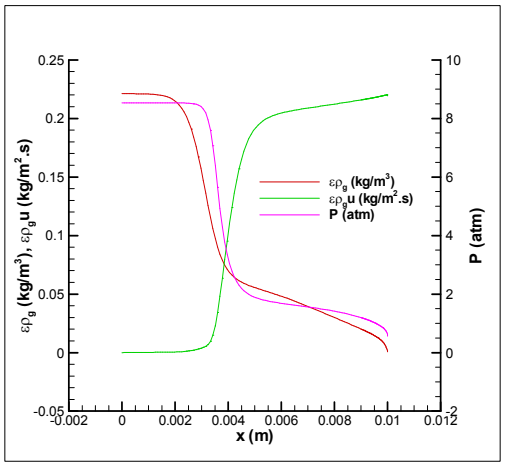

a) Gas density, gas momentum and pressure

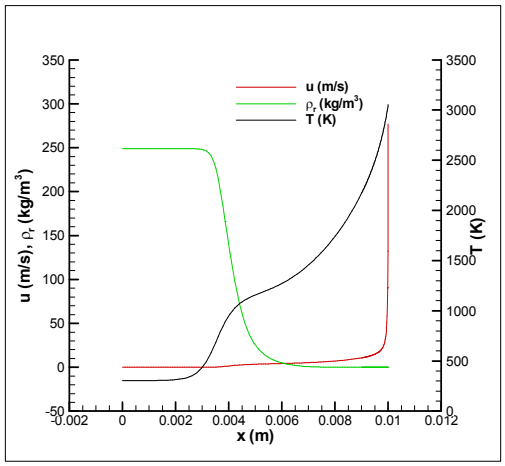

b) Gas velocity, resin density and temperature

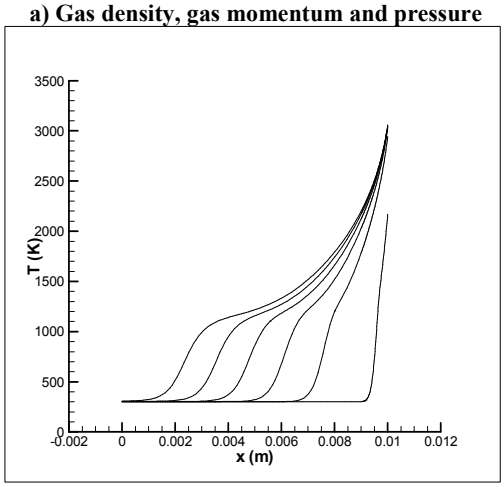

c) Temperature distribution at different times

Figure 8. Top two plots a) and b) show all solution variables for Arc-jet case with non-zero diffusion term at time = 4 sec. a) shows gas density, $\varepsilon\rho_g$, gas momentum, $\varepsilon\rho_g u$ and pressure, P; b) shows gas velocity, u, resin density, ρ_r, and temperature, T; and c) shows temperature distribution within the domain at times = 0.1, 1, 2, 3, 4, and 5 sec.

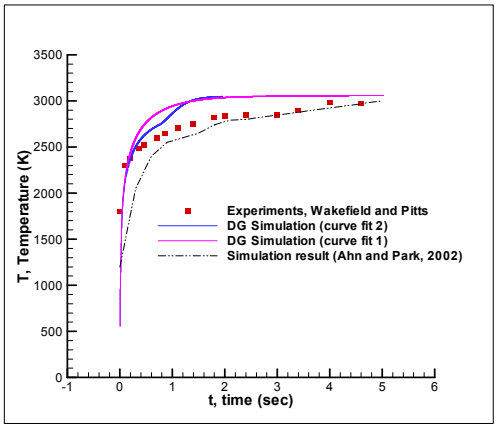

Figure 9. Temporal surface temperature variation for non zero D and 2002 paper

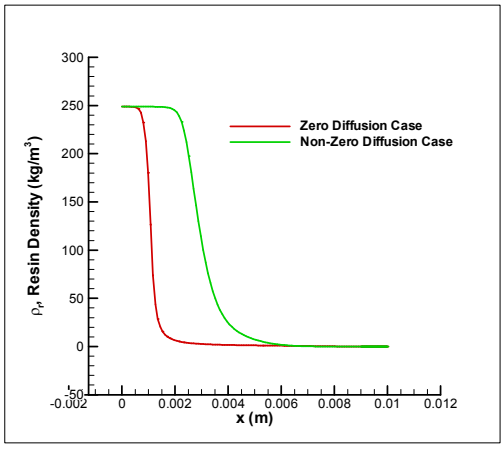

a) Resin Density

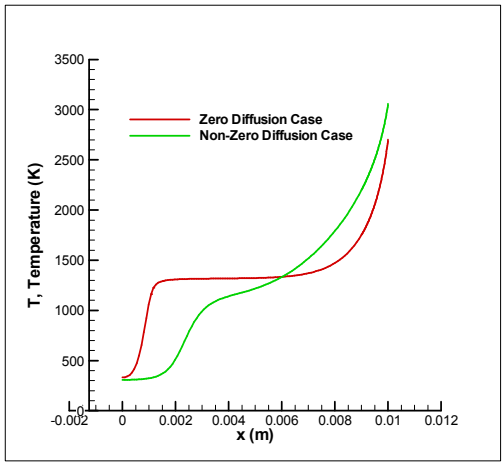

b) Temperature

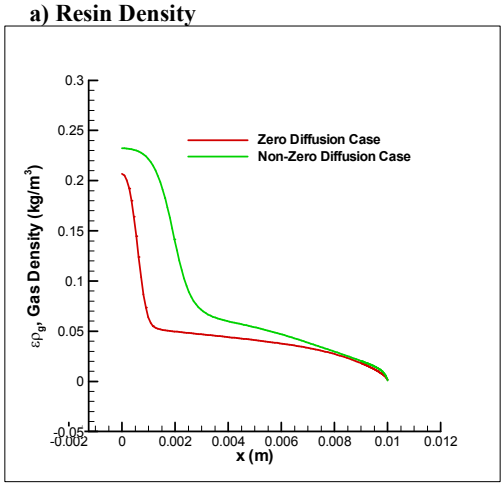

c) Gas density

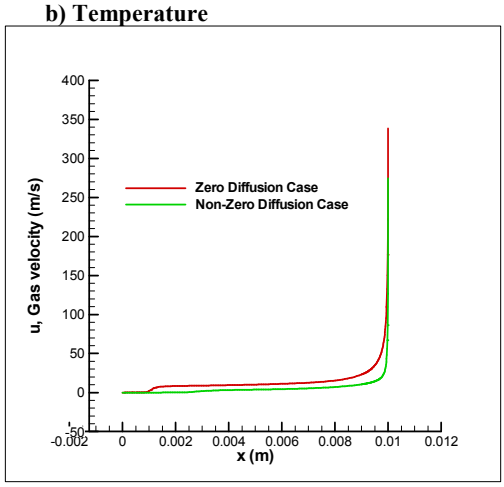

d) Gas velocity

Figure 10. Comparison plots for cases with zero and non-zero diffusion coefficients for a) resin density, b) temperature, c) gas density and d) gas velocity at time, t = 5 sec. We can notice for same heat in-flux and total time, lesser material is used with non-zero diffusion case than with zero diffusion case.

C. 2-D Discontinuous Galerkin application to Double Mach Reflection Problem

In our attempt to develop 2-D capability for discontinuity Galerkin method, we applied this code to problems of advection and Burgers equations and double mach reflection problem. For time-integration we have used implicit method (BDF -1 or Backward Difference Formula). Here we only present results for double mach reflection. This is a well known problem, and has been attempted analytically, experimentally and numerically. In the field of DG methods, it was solved in [6]. We try this problem, as a first step into building a 2-D DG capability in our in-house code, MIG. Schematic of this problem (taken from [26]) is given in Fig. 11.

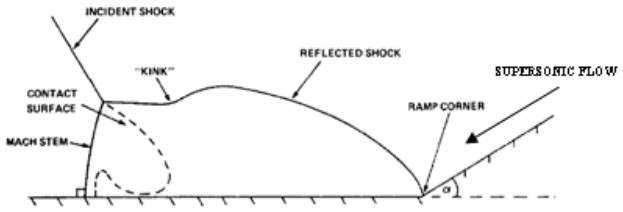

Figure 11. Schematic of 2-D double mach reflection problem (taken from [26])

Here supersonic flow meets the ramp (horizontal line in Fig. 11) at an angle of α, due to which the incoming shock is reflected from this compressive ramp, and this interaction is referred to as double mach reflection. For boundary conditions, and domain information please refer to [26]. Since this problem has a strong shock and due to absence of an external artificial dissipation mechanism in our scheme, we get overshoots and undershoots across the shock; this causes the density and total energy to take negative values near shock. In our code, we limit values of density and total energy to their minimum physically possible values. By this we have been able to get results for k = 1 (linear polynomial approximation) for DG method. For higher k (>= 2), the jumps across shock become steeper and we get convergence issues, so we haven't been able to get solutions for full run time for higher k. In order to resolve these issues, we are working on implementing artificial dissipation scheme for removing these oscillations and as shown in [12], with higher k, we should expect more accurate solutions.

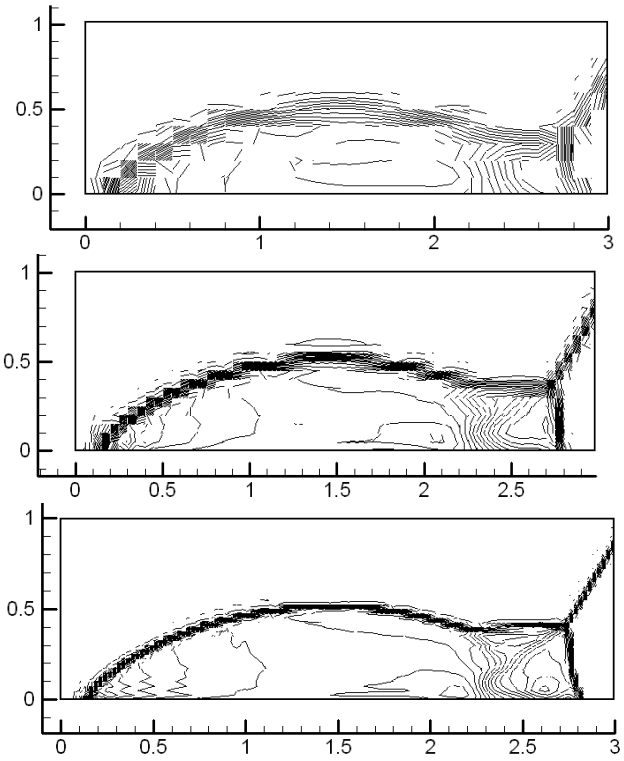

Figure 12. Density contours obtained for 40 X 10, 80 X 20, and 160 X 40 mesh (arranged from top to bottom) and k = 1 (linear polynomial approximations), time-step for above simulations is 1.0e-04 sec, and results are shown at t = 0.2 sec

Fig. 12 shows density contours for gas density at t = 0.2 sec. For these simulations we use time-step of 1.0e-4 sec, and the results are shown for 40 X 10, 80 X 20, and 160 X 40 mesh and k = 1, i.e. linear polynomial approximation. The domain dimensions are 4 m in x-direction and 1 m in y-direction. Initial location of shock is at (1/6, 0), and aligned at 60^o to x-axis. We can easily notice that solution quality clearly improves with refined mesh, but due to lack of artificial dissipation for this problem, the jumps across the shock become more severe and hence solution becomes difficult to converge. The solution contours are comparable to other published results of this problem, but with higher mesh we can observe oscillatory nature of density contours. At very coarse mesh, this is not observed, but many fine flow features become visible with finer mesh. Also with k = 2, i.e. quadratic polynomial approximation jumps become more severe and simulations hard to converge.

Convergence results for double mach reflection problem are also shown in figure given below, in Fig. 13. Data points for both L2 and L∞ norm of density are plotted for all the three meshes considered above, along with their linear fit, and it can be seen easily that the simulations converge to a fixed solution with the given three meshes. Norms are plotted against mesh measure, which is the uniform edge thickness of the meshes used, which are same for x and y axis.

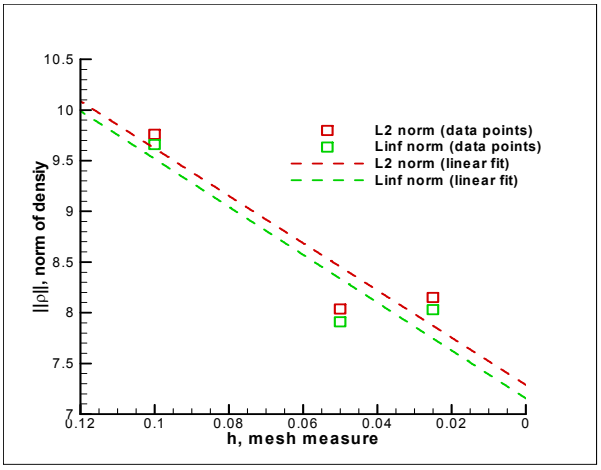

Figure 13. Mesh refinement study for the double mach reflection problem, where norm of the density is plotted against the mesh measure, h

V. Conclusion & Future Work

An implicit discontinuous Galerkin method to solve thermal ablation is introduced and the results are benchmarked with the previously reported results. We are able to achieve near quadratic convergence using numerically evaluated jacobians in Newton Raphson scheme. Two cases with and without the diffusion term were compared and it was found that the modeling of the dynamics of pyrolysis gas does affect the net thermal response of the TPS. The case with $D \neq 0$ has more diffused profiles for pressure, density and temperature and hence the pyrolysis front travels at a slower speed in this case than for $D = 0$. Consequently, lower amount of resin material is used up with $D \neq 0$. Hence, neglecting the diffusion term will lead to over prediction of TPS mass, which means increased fuel cost for the space mission. So, we see that modeling of motion of pyrolysis gas is very crucial in accurately deciding the net response of TPS, and this is neglected in many numerical codes on in-depth thermal ablation. Pyrolysis gas was considered to be in thermal equilibrium in current work, and we will explore avenues for considering finite rate reaction in our future work. Some modeling inconsistencies in between [1] and [2] are also noted and this will be further investigated. To extend our current work to higher dimensions, we are building a 2-D DG capability, and as a part of our ongoing work in this area, we have shown results for double mach reflection problem. As a next step, we plan to apply artificial dissipation to this 2-D double mach reflection problem, which will solve the problem of capturing shock, without spurious oscillations of jumps (overshoots and undershoots at discontinuities).

Acknowledgments

This work was partially supported by Florida Center of Advanced Aero-Propulsion (FCAAP) and the department of Mechanical & Aerospace Engineering at the University of Florida, Gainesville.

References

[1]H. – K. Ahn, C. Park, K. Sawada, "Dynamics of Pyrolysis Gas in Charring Materials Ablation", *36th Aerospace Sciences Meeting & Exhibit,* A98-16086, 12 – 15 January, 1998

[2]H. – K. Ahn, C. Park, K. Sawada, "Response of Heatshield Material at Stagnation Point of Pioneer-Venus Probes", *Journal of Thermophysics and Heat Transfer,* 16(3), July – September 2002

[3]B. Cockburn, S. Y. Lin and C.-W. Shu, "TVB Runge-Kutta local projection discontinuous Galerkin finite element method for conservation laws III: One dimensional systems", *J. Comput. Phys.,* 84:90-113, 1989

[4]B. Cockburn and C.-W. Shu, "TVB Runge-Kutta local projection discontinuous Galerkin finite element method for scalar conservation laws II: General framework", *Math. Comput.,* 52:411-435, 1989

[5]B. Cockburn, S. Hou, and C.-W. Shu, "TVB Runge-Kutta local projection discontinuous Galerkin finite element method for conservation laws IV: The multidimensional case", *Math. Comput.,* 54:545-581, 1990

[6]B. Cockburn and C.-W. Shu, "TVB Runge-Kutta local projection discontinuous Galerkin finite element method for conservation laws V: Multidimensional systems", *J. Comput. Phys.,* 141:199-224, 1998

[7]F. Bassi and S. Rebay, "A high order accurate discontinuous finite element method for the numerical solution of compressible Navier-Stokes equation", *J. Comput. Phys.,* 131(2), 1997

[8]B. Cockburn and C.-W. Shu, "The local discontinuous Galerkin method for time-dependent convection-diffusion systems", *SIAM J. Numer. Anal.,* 35:2440-2463, 1998

[9]D. N. Arnold, F. Brezzi, B. Cockburn and D. Marini, "Unified analysis of discontinuous Galerkin methods for elliptic problems", *SIAM J. Numer. Anal.,* 39(5):1749-1779, 2001

[10]B. Cockburn, "Discontinuous Galerkin Methods for Convection-dominated Problems", *Lecture Notes in Computational Science and Engineering,* Vol. 9, High-Order Methods for Computational Physics

[11]P.-O. Persson, J. Peraire, "An Efficient Low Memory Implicit DG Algorithm for Time Dependent Problems", *Proc. of the 44th AIAA Aerospace Sciences Meeting and Exhibit*, AIAA-2006-113, 2006

[12]P.-O. Persson, J. Peraire, "Sub-Cell Shock Capturing for Discontinuous Galerkin Methods", *Proc. of the 44th AIAA Aerospace Sciences Meeting and Exhibit*, AIAA-2006-112., 2006

[13]P.-O. Persson, "Scalable Parallel Newton-Krylov Solvers for Discontinuous Galerkin Discretizations", *Proc. of the 47th AIAA Aerospace Sciences Meeting and Exhibit*, AIAA-2009-606, 2009

[14]J. Peraire and P.-O. Persson, "The Compact Discontinuous Galerkin (CDG) Method for Elliptic Problems", *SIAM J. Sci. Comput.*, Vol. 30, No. 4, pp. 1806-1824, 2008

[15]P.-O. Persson and J. Peraire, "Newton-GMRES preconditioning for Discontinuous Galerkin Discretizations of the Navier-Stokes Equations", *SIAM J. Sci. Comput.*, Vol. 30, No. 6, pp. 2709-2733, 2008

[16]S. Roy and B. P. Pandey, "Numerical Investigation of a Hall Thruster Plasma", *Physics of Plasmas*, 2002, v9, n9, p. 4052-60

[17]S. Roy and D. Gaitonde, "Radio Frequency Induced Ionized Collisional Flow Model for Application at Atmospheric Pressures", *Journal of Applied Physics*, v96, n5, p. 2476-2481, 2004

[18]S. M. Cooper, B. Cruden, M. Meyyappan, R. Raju and S. Roy, "Gas Transport Characteristics through a Carbon Nanotubule", *Nano Letters*, 2004

[19]S. Kapadia, S. Roy and J. Heidmann, "First Hybrid Turbulence Modeling for Turbine Blade Cooling", *Journal of Thermophysics and Heat Transfer*, 2004

[20]R. M. Wakefield and W. C. Pitts, "Analysis of the Heat-Shield Experiment on the Pioneer-Venus Entry Probes", *AIAA 1980-1494*, July 1980

[21]D. G. Goodwin, CANTERA, *Division of Engineering and Applied Science, California Institute of Technology,* www.cantera.org

[22]J. R. Phillips, "Online Curve Fitting and Surface Fitting Web Site", www.zunzun.com

[23]http://www.km.kongsberg.com/

[24]A. Bhatia and S. Roy, "Modeling the motion of pyrolysis gas through charring ablating material using Discontinuous Galerkin finite elements", *48th AIAA/ASM Including the New Horizons Forum and Aerospace Exposition,* AIAA 2010-982, 4-7 January 2010

[25]B. Landmann, "A parallel discontinuous Galerkin code for the Navier-Stokes and Reynolds-averaged Navier-Stokes equations", *Ph.D. thesis,* University of Stuttgart, Germany, 2008

[26]P. Collela, H. M. Glaz, "Efficient Solution Algorithms for the Riemann Problem for Real Gases", *Journal of Computational Physics,* 59, 264–289, 1985

[27]N. C. Nguyen, P. -O. Persson, J. Peraire, "RANS Solutions Using High Order Discontinuous Galerkin Methods", *Proc. of the 45th AIAA Aerospace Sciences Meeting and Exhibit*, AIAA-2007-914, January 2007

[28]A. Bhatia, S. Roy, R. Gosse, "Application of Discontinuous Galerkin Methods to Thermal Ablation", *Journal of Computational Physics,* (submitted for review, 2010)

[29]E.F. Toro, "Riemann Solvers and Numerical Methods for Fluid Dynamics: A Practical Introduction," Springer, 2nd edition (1999).